Letter

Nodal-line driven anomalous susceptibility in ZrSiS

Bruno Gudac,[1] Markus Kriener,[2] Yuriy V. Sharlai,[3] Mihovil Bosnar,[4,5] Filip Orbanić,[1] Grigorii P. Mikitik,[3] Akio Kimura,[6,7] Ivan Kokanović,[1] and Mario Novak[1,*]

[1]*Department of Physics, Faculty of Science, University of Zagreb, 10000 Zagreb, Croatia*
[2]*RIKEN Center for Emergent Matter Science (CEMS), Hirosawa 2-1, Wako-shi, Saitama 351-0198, Japan*
[3]*B. Verkin Institute for Low Temperature Physics & Engineering, Ukrainian Academy of Sciences, Kharkiv 61103, Ukraine*
[4]*Division of Theoretical Physics, Ruđer Bošković Institute, 10000 Zagreb, Croatia*
[5]*Donostia International Physics Center, 20018 Donostia-San Sebastian (Gipuzkoa), Spain*
[6]*Graduate School of Advanced Science and Engineering, Hiroshima University, Higashi-Hiroshima 739-8526, Japan*
[7]*Graduate School of Science, Hiroshima University, Higashi-Hiroshima, Hiroshima 739-8526, Japan*

(Received 21 March 2022; revised 31 May 2022; accepted 1 June 2022; published 29 June 2022)

We demonstrate a unique approach to test the signature of the nodal-line physics by thermodynamic methods. By measuring magnetic susceptibility in ZrSiS we found an intriguing temperature-driven crossover from dia- to paramagnetic behavior. We show that the anomalous behavior represents a real thermodynamic signature of the underlying nodal-line physics through the means of chemical pressure (isovalent substitution of Zr for Hf), quantum oscillations, and theoretical modeling. The anomalous part of the susceptibility is orbital by nature, and it arises due to the vicinity of the Fermi level to a degeneracy point created by the crossing of two nodal lines. Furthermore, an unexpected Lifshitz topological transition at the degeneracy point is revealed by tuning the Fermi level. The present findings in ZrSiS give an attractive starting point for various nodal-line physics-related phenomena to be tested by thermodynamic methods in other related materials.

DOI: 10.1103/PhysRevB.105.L241115

Dirac materials are characterized by a linear dispersion of energy-momentum curves near the Fermi energy. Due to the linearity of the dispersion, quasiarticles generically exhibit low effective masses and high mobilities [1]. Dirac states have been realized and studied in plenty of materials and new fascinating phenomena such as Fermi arcs and chiral anomalies have been revealed [2,3]. Under high-magnetic fields, these materials exhibit remarkably different behavior than conventional matter. The Landau levels become nonequidistant with a square root magnetic field dependence [4]. This feature is often used to verify the Dirac nature of a material experimentally [5,6].

The magnetic susceptibility, a low-field limit of the magnetic response function, in Dirac and nodal-line systems, shows unique properties due to the existence of band touching degeneracy points and/or lines [7–11]. For example, in contrast to ordinary metals, in Dirac materials the orbital (Landau) susceptibility diverges as the Fermi energy approaches the degeneracy point at low temperatures [7–10]. The orbital susceptibility originates from the dynamics of the Bloch electrons. It incorporates interband magnetic field mixing, and it is summed over Bloch states [12,13]. Although it possesses unique fingerprints, the susceptibility of novel Dirac systems has not been widely studied experimentally [14–16].

In this letter, we present a chemical pressure study of the magnetic susceptibility of the nodal-line Dirac semimetal ZrSiS. The susceptibility exhibits an anomalous temperature dependence pointing towards a unique thermodynamic signature of nodal-line physics. The anomaly arises due to the Fermi level being located sufficiently close to the degeneracy point formed by the crossing of two nodal lines.

ZrSiS crystallizes in a tetragonal square-net crystal structure with nonsymmorphic $P4/nmm$ (129) symmetry [17]. It is one of the reported topological nodal-line semimetals and has been the most extensively studied among a range of different nodal-line materials [18–26]. In ZrSiS, there are two types of nodal lines. Topologically protected nodal lines, nonsymmorphic symmetry protection, are positioned with about 1eV below the Fermi level and are not significant for our experimental findings [19,20]. However, close to the Fermi level, another set of nodal lines is found. Those nodal lines form a cage-like structure, see the inset to Fig. 1(c). They are not topologically protected, only $C4v$ symmetry is present, and are thus prone to the opening of a gap that is induced by the spin-orbit (SO) interaction. Due to the relatively weak SO coupling, the resulting gap is small [27].

Angle-resolved-photoemission spectroscopy and high magnetic field studies together with first-principle calculations yield a reasonably well understood Fermi surface (FS) [22,25,28,29]. The FS is wrapped around the cagelike nodal lines. It consists of a pair of strongly anisotropic electron and hole pockets with open orbits along the k_z direction [22]. At the Fermi level only the Dirac-like bands are present, while the so-called "trivial" bands are well away [19].

Recent high-pressure studies reported a change in the Berry phase of the quantum oscillations (QOs), indicating the possibility of a topological phase transition (TPT). In Ref. [30]

*mnovak@phy.hr

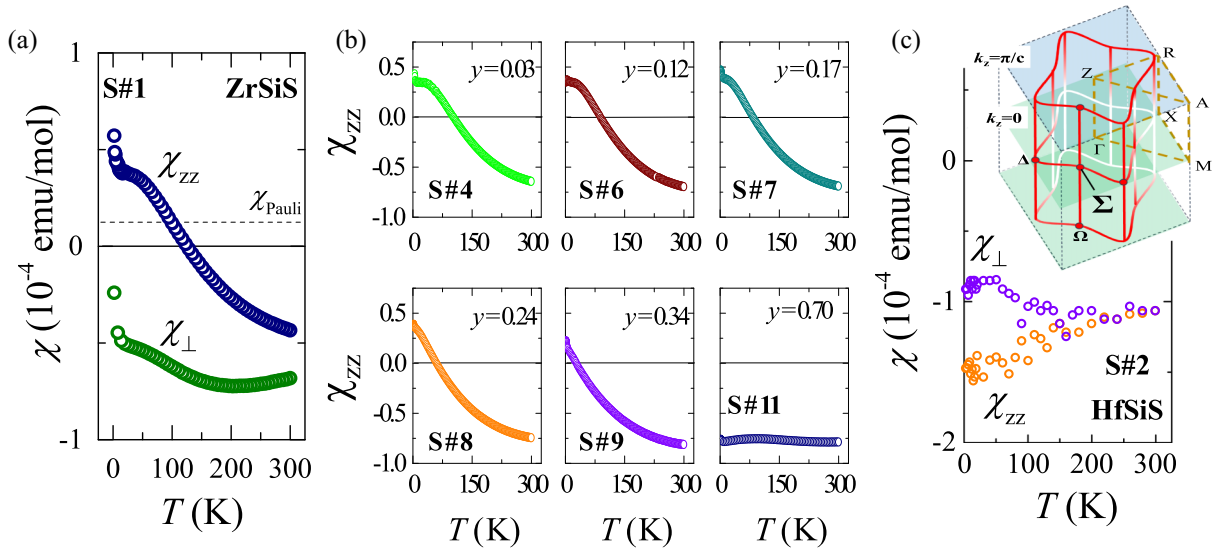

FIG. 1. Temperature (T) dependent magnetic susceptibility of $Zr_{1-y}Hf_ySiS$ taken at 1 T for various Hf concentrations y. (a) Out-of-plane χ_{zz}, along [001], and in-plane $\chi_\perp$ susceptibility of ZrSiS. χ_{zz} has a strong anomalous T dependence with unexpected change in the susceptibility from diamagnetic at high T to paramagnetic at low T. By contrast $\chi_\perp$ exhibits a weak T dependence with an impurity tail at low T. χ_{Pauli} (dashed line) indicates the free-electron Pauli paramagnetic contribution as estimated from the specific heat measurements. (b) χ_{zz} for different y: Upon increasing chemical pressure the sign change in χ_{zz} shifts toward lower T. For $y > 0.24$ the low-T saturation of χ_{zz} vanishes. At high doping $y = 0.7$, χ_{zz} flattens and remains diamagnetic in the whole T range examined. (c) χ_{zz} and $\chi_\perp$ for HfSiS exhibit a conventional, almost isotropic and week T dependence. (Inset) Schematics of the cage of nodal lines in the 1st Brillouin zone. The intersecting nodal-line of interest Σ is located along the Γ-M direction.

the authors report the possibility of a TPT at pressures as low as 0.5 GPa due to a phase change in the QO frequency mode $F_{\delta 2}$, this paper's notation. Additionally, the authors in Ref. [31] report another TPT at around 7 GPa with a transition detected in the QO frequency mode F_α, again in the notation used here. In contrast, in our study, we observe a significantly different qualitative behavior, even in the low-chemical pressure limit, i.e., at low Hf concentrations (y). We have detected two possible chemical-pressure-driven Lifshitz transitions in the low-frequency spectrum of the QOs. The first transition is associated with the emergence of a new frequency F_ψ around $y = 0.24$. The second transition is observed at around $y \approx 0.34$ as indicated by the disappearance of the pocket $F_{\delta 1}$. The notable difference between the results of hydrostatic and chemical pressure could be traced back to a different compression of the crystal lattice: In the case of chemical substitution of Zr by Hf Vegard's law is obeyed, i.e., the tetragonal lattice ratio $c/a = 2.273$ is practically constant across $Zr_{1-y}Hf_ySiS$, while that is not the case for the hydrostatic pressure where the ratio is reduced by increasing pressure [17,31].

Single crystals of $Zr_{1-y}Hf_ySiS$ were grown by chemical vapor transport starting from a polycrystalline mixture of high-purity elements and iodine as a transport agent. With optimized growth conditions, well shaped prismatic crystals of several mm^3 weighing 20–30 mg that are ideal for magnetization studies were observed. To get information on the concentration and homogeneity of the doped Hf atoms, the samples were characterized by employing an electron probe micro analysis and x-ray diffraction (XRD). XRD patterns show a systematic shift of the (002) peak upon increasing the Hf concentration without any traces of segregation, indicating a homogeneous Zr-Hf solid solution.

Magnetic susceptibility (χ) vs temperature (T) was measured using a Quantum Design MPMS superconducting quantum interference device magnetometer from 300 to 1.8 K in the linear response regime at a field of 1T. The out-of-plane susceptibility χ_{zz} was measured along the [001] direction, and the in-plane susceptibility $\chi_\perp$ was measured perpendicular to [001]. There was no difference in the sample response between field-cooled and zero-field-cooled measurements. The de Haas–van Alphen oscillations were measured in the [001] direction in the field range -7 T to 7 T at several different temperatures in order to estimate the quasiparticle effective mass. The QOs were not significantly damped upon increasing the Hf concentration indicating a small level of atomic substitution-induced disorder.

Figure 1 summarizes magnetic susceptibility data of $Zr_{1-y}Hf_ySiS$. For $y = 0$, there is a strong anisotropy between χ_{zz} and $\chi_\perp$, cf. Fig. 1(a). Moreover, χ_{zz} has an unconventional steplike temperature dependence with a T-driven transition from a dia- to paramagnetic state and saturation towards the lowest T, whereas $\chi_\perp$ is relatively weakly T dependent. The low-T paramagnetism of ZrSiS is much stronger than expected for free-electron Pauli susceptibility term χ_{Pauli} as derived from the specific heat density of states. The small upturns at the lowest temperatures (below $\sim$10K) originate from paramagnetic impurities of 0.01%. On the other hand, the end compound HfSiS [Fig. 1(c)] exhibits more isotropic and T-independent susceptibility, which is more in line with expectations for conventional materials. To get better insight

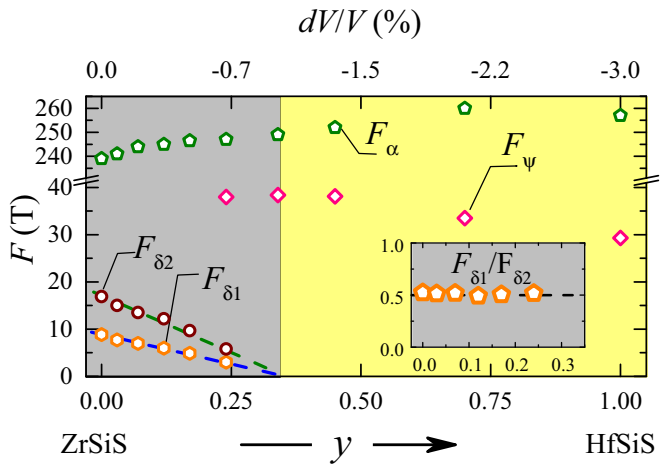

FIG. 2. Phase diagram of QO frequency vs Hf concentration y in $Zr_{1-y}Hf_ySiS$ along the crystallographic [001] direction. Two Lifshitz transitions in the low-frequency spectrum are identified: A new pocket with frequency F_ψ emerges at around $y = 0.24$, and an electron pocket with frequency $F_{\delta 1}$ ($F_{\delta 2}$) vanishes at $y \approx 0.34$ (as estimated from linear interpolations - green and blue dashed lines, respectively). Clearly, the low-frequency QOs seen in [001] direction for ZrSiS and HfSiS are topologically not connected. On the other hand the hole-pocket frequency F_α increases with y and is continuously connected between $y = 0$ and $y = 1$. The inset shows the ratio of the frequencies $F_{\delta 1}/F_{\delta 2}$ which does not change with y. The dashed lines are guide to the eye.

into the unconventional behavior of $\chi_{zz}(T)$ observed for $y = 0$ we introduce positive chemical pressure by replacing Zr with isovalent Hf. Respective susceptibility measurements for selected y are shown in Fig. 1(b). Upon increasing the Hf content, the steplike feature indicative of the transition from dia- to paramagnetic behavior shifts to lower-T. For $y = 0.34$ the susceptibility starts to deviate from the steplike behavior, although the dia- to paramagnetic transition is still present. However, it is significantly weaker and no longer saturates towards low T, indicating that the effect responsible for this unconventional behavior is suppressed by chemical pressure. At $y = 0.7$ χ_{zz} is T independent and remains diamagnetic.

To investigate whether the unconventional behavior of χ_{zz} is linked to the change of the FS shape we have performed QO measurements for $B||[001]$. Figure 2 shows the QO frequencies as a function of chemical pressure. It can be seen that the frequency F_α associated with a hole-pocket orbit in the $Z - R - A$ plane smoothly increases with y. On the other hand, in the low-frequency part of the diagram two Lifshitz transition can be identified. The first one is an ordinary $2\frac{1}{2}$ [32] Lifshitz transition associated with the appearance of a new pocket with frequency F_ψ. It is detected at around $y = 0.24$ and possibly could be ascribed to the appearance of an electron pocket at the Γ point as predicted by first-principles calculations in HfSiS [18].

The second Lifshitz transition is associated with the continuously traced disappearance of the oscillations with frequency $F_{\delta 1}$ at around $y = 0.3$. As shown in the inset to Fig. 2, the ratio of $F_{\delta 1}$ and $F_{\delta 2}$ is constant and equal to 0.5. Thus we believe $F_{\delta 2}$ originates from the second harmonic response of the QOs and is not indicative of an additional pocket. Interestingly, the disappearance of $F_{\delta 1}$ coincides with the disappearance of the anomalous steplike behavior in the susceptibility: For $y \leqslant 0.24$, the value of the frequency $F_{\delta 1}$ decreases with y. At the same time the sign change in χ_{zz} from diamagnetic to paramagnetic shifts to lower T and for $y = 0.34$ $F_{\delta 1}$ cannot be detected anymore, although $\chi_{zz}(T)$ still exhibits a small sign change. However, the latter deviates considerably from the steplike behavior observed for smaller y.

$F_{\delta 1}$ seems to be produced by the FS cross section located near the Σ point [28,33], a degeneracy point at which the two nodal lines intersect [19,22], see Fig. 1(c). We can show that the observed temperature dependence of the magnetic susceptibility is also caused by the electron states in the vicinity of the Σ point. Neglecting the spin-orbit interaction, the dispersion of the two contacting bands "c" and "v" in the vicinity of this crossing point can be approximately described by the following expression [33,34]:

$$\varepsilon_{c,v}(\mathbf{k}) \approx B_2 k_2^2 + B_3 k_3^2 \pm \left[(v_F k_1)^2 + \beta^2 k_2^2 k_3^2\right]^{1/2}, \qquad (1)$$

where v_F, B_1, B_2, β are constant parameters of the spectrum, all the quasimomenta k_1, k_2, k_3 are measured from the Σ point, and $\varepsilon_{c,v}$ are measured from the energy of this point, ε_Σ. The k_1 axis coincides with the twofold symmetry axis Γ-M along which the crossing point Σ is located. The k_2 and k_3 axes are along the tangents to the nodal lines crossing the Σ point (in particular, the k_3 axis coincides with the z axis); see Fig. 1. According to Ref. [34], electron states in the vicinity of such a crossing point really can lead to an unusual anomaly in the magnetic susceptibility if the Fermi energy (E_F) is close to ε_Σ. One has the following expression for the total magnetic susceptibility in this case [34,35]:

$$\chi_{zz} = \chi_0 + \Delta\chi[1 + \exp(-E_F/k_B T)]^{-1}, \qquad (2)$$

where E_F is measured from the energy of the crossing point, and χ_0 is the magnetic susceptibility produced by the electron states lying far away from this point. The constant $\Delta\chi$ is defined by the parameters of dispersion relation (1), and at $|\lambda| \equiv 4|B_2 B_3|/\beta^2 \ll 1$, it has the form [34,35]:

$$\Delta\chi \approx -4\frac{e^2}{6\pi^2\hbar c^2}\frac{v_F\beta}{B_3}, \qquad (3)$$

where we have taken into account that in the case of ZrSiS four Σ points exist in the first Brillouin zone.

Formula Eq. (2) with the addition of a $1/T$ term that is important below 10 K in order to account for the localized magnetic impurities reproduces the T behavior of χ_{zz} extremely well in the low-y region, Fig. 3(a), if the chemical potential E_F monotonically decreases with y, tending to the energy of the Σ point, Fig. 3(b). The parameter $\Delta\chi$ remains practically constant with changing y, Fig. 3(d), which in the agreement with the natural assumption that the parameters v_F, β, and B_3 are constant or their variation is proportionally small to the small y [36].

For $y > 0.3$, formula (2) ceases to fit the experimental data. This failure of Eq. (2) at $E_F \sim 10$ meV is due to the neglect of the spin-orbit interaction in deriving this formula. Note that the magneto-optical spectroscopy [27] shows that the gap in

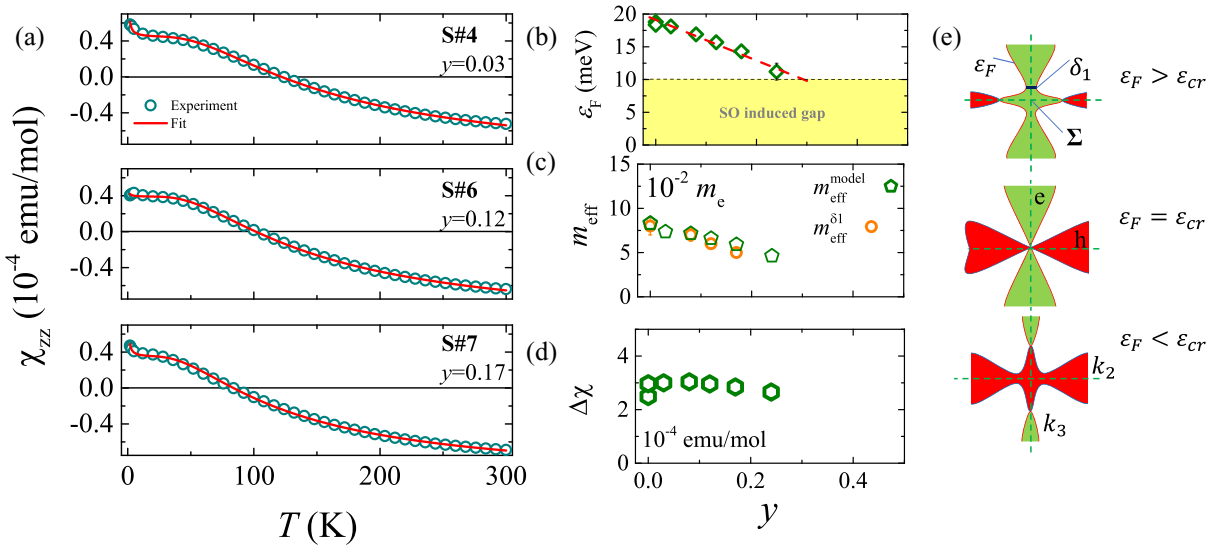

FIG. 3. (a) Fit of Eq. (2) to experimental $\chi_{zz}(T)$ for samples $y = 0.03$, 0.12, and 0.17 including localized paramagnetic impurity contributions responsible for the low-T upturn. The model fairly well captures the experimental data in the whole measured T range. (b) Fermi energy (E_F) measured from the nodal-line crossing point as a function of y. Below ≈10 meV our model breaks down due to the SO-interaction induced gap at the nodal line. (c) Effective mass $m_{\rm eff}^{\delta 1}$ as estimated from QO of the $\delta 1$ orbital compared with the effective mass $m_{\rm eff}^{\rm model}$ as a function of y. (d) Almost constant value of $\Delta\chi$ from Eq.(2) as a function of y indicates that the FS around the crossing points is not strongly modified for low levels of y. (e) Schematic drawing of the Fermi surface with self-intersecting orbitals near the degeneracy point Σ based on the model Eq.(1) (parameters $B_1 = -B_2$ and $\lambda < 0$). By tuning the Fermi energy the system undergoes a nonstandard Lifshitz transition characterized by a change in the configuration of the e-h pockets and direction of the intersecting orbitals.

the spectrum induced by this interaction is of the order of $2\Delta \approx 26$ meV, and hence is comparable with the limiting value of $E_F \sim 10$ meV. It is clear that at such a low value of E_F, one cannot neglect the spin-orbit gap.

Visible y correlation between $F_{\delta 1}$ and the Fermi-level E_F extracted from the magnetic susceptibility indicate that the susceptibility and the frequency $F_{\delta 1}$ are really determined by the same part of the FS near the Σ point. To support this conclusion quantitatively, in Fig. 3(c) we compare experimental QO effective masses with the one predicted by the model. The model predicts the effective mass of the cyclotron orbit around the neck of the electron tubelike pocket near the Σ to be $m_{\rm eff}^{\rm model} = 3\hbar eF/2E_{\rm F}$, where F is the frequency of QOs of the neck orbitals, and E_F is the Fermi energy of the pocket [33]. Using the above-presented values yields effective masses that are in excellent agreement with those obtained from the QOs. The model can be further extended by taking into account a spectrum with the spin-orbit gap [37], suggesting that the gap does not exceed 10 meV. For $y > 0.3$, E_F is likely located inside the spin-orbit gap at the Σ point, and so the gap effects become important. Indeed, if we check the FS shape obtained by the first-principles calculations for HfSiS we see a FS with nonoccupied states near the Σ point, see Ref. [38] and the Supplemental Material [39].

In conclusion, we present a comprehensive study of the anomalous magnetic susceptibility of ZrSiS, which arises due to the proximity of the Fermi energy to the degeneracy point formed by intersecting nodal lines. The anomalous susceptibility provides a rare opportunity to observe nodal-line physics by thermodynamic methods. Introduction of chemical pressure by replacing Zr with Hf in $Zr_{1-y}Hf_ySiS$ allows one to trace the evolution of the susceptibility anomaly and to test the model of the electronic spectrum around the Σ degeneracy point. The model predicts a temperature-dependent orbital magnetization which is in excellent agreement with the experimental data for Hf concentrations $y \leqslant 0.24$. Also, the estimated spin-orbit gap at the nodal line matches the gap value obtained from the optical spectroscopy measurements. Moreover, the effective masses as estimated from quantum oscillations are in excellent agreement with those yielded within our theoretical model. The phase diagram of $Zr_{1-y}Hf_ySiS$ reveals two different Lifshitz transitions, indicating a very rich topology-related physics which could also manifest in other closely related nodal-line systems [17,18].

This work was supported by the CSF under Project No. IP 2018 01 8912 and the CeNIKS project cofinanced by the Croatian Government and the EU through the European Regional Development Fund-Competitiveness and Cohesion Operational Program (Grant No. KK.01.1.1.02.0013). We thank G. Eguchi for the specific heat measurements and J.R. Cooper for giving constructive suggestions. A.K. acknowledges financial support from KAKENHI (Grants No. 17H06138 and No. 18H03683). M.N. acknowledges the financial support from JSPS International Fellowships for Research in Japan.

[1] A. K. Geim and K. S. Novoselov, The rise of graphene, Nat. Mater. **6**, 183 (2007).

[2] N. P. Armitage, E. J. Mele, and A. Vishwanath, Weyl and Dirac semimetals in three-dimensional solids, Rev. Mod. Phys. **90**, 015001 (2018).

[3] J. Xiong, S. K. Kushwaha, T. Liang, J. W. Krizan, M. Hirschberger, W. Wang, R. J. Cava, and N. P. Ong, Evidence for the chiral anomaly in the Dirac semimetal Na_3Bi, Science **350**, 413 (2015).

[4] J. W. McClure, Diamagnetism of Graphite, Phys. Rev. **104**, 666 (1956).

[5] P. Plochocka, C. Faugeras, M. Orlita, M. L. Sadowski, G. Martinez, M. Potemski, M. O. Goerbig, J. N. Fuchs, C. Berger, and W. A. De Heer, High-Energy Limit of Massless Dirac Fermions in Multilayer Graphene Using Magneto-Optical Transmission Spectroscopy, Phys. Rev. Lett. **100**, 087401 (2008).

[6] E. Martino, I. Crassee, G. Eguchi, D. Santos-Cottin, R. D. Zhong, G. D. Gu, H. Berger, Z. Rukelj, M. Orlita, C. C. Homes, and A. Akrap, Two-Dimensional Conical Dispersion in $ZrTe_5$ Evidenced by Optical Spectroscopy, Phys. Rev. Lett. **122**, 217402 (2019).

[7] G. P. Mikitik and I. V. Svechkarev, Giant Anomalies of magnetic-susceptibility due to energy-band degeneracy in crystals, Fiz. Nizk. Temp. **15**, 295 (1989) [Sov. J. Low Temp. Phys. **15**, 165 (1989)].

[8] G. P. Mikitik and Y. V. Sharlai, Magnetic susceptibility of topological nodal semimetals, Phys. Rev. B **94**, 195123 (2016).

[9] M. Koshino and T. Ando, Diamagnetism in disordered graphene, Phys. Rev. B **75**, 235333 (2007).

[10] M. Koshino and I. F. Hizbullah, Magnetic susceptibility in three-dimensional nodal semimetals, Phys. Rev. B **93**, 045201 (2016).

[11] Y. Ominato and K. Nomura, Spin susceptibility of three-dimensional Dirac-Weyl semimetals, Phys. Rev. B **97**, 245207 (2018).

[12] M. Ogata and H. Fukuyama, Orbital magnetism of Bloch electrons I. General formula, J. Phys. Soc. Jpn. **84**, 124708 (2015).

[13] H. Fukuyama, Theory of orbital magnetism of Bloch rlectrons: Coulomb interactions, Prog. Theor. Phys. **45**, 704 (1971).

[14] A. Raoux, M. Morigi, J.-N. Fuchs, F. Piéchon, and G. Montambaux, From Dia- to Paramagnetic Orbital Susceptibility of Massless Fermions, Phys. Rev. Lett. **112**, 026402 (2014).

[15] N. L. Nair, P. T. Dumitrescu, S. Channa, S. M. Griffin, J. B. Neaton, A. C. Potter, and J. G. Analytis, Thermodynamic signature of Dirac electrons across a possible topological transition in $ZrTe_5$, Phys. Rev. B **97**, 041111(R) (2018).

[16] Y. Fuseya, M. Ogata, and H. Fukuyama, Transport properties and diamagnetism of dirac electrons in bismuth, J. Phys. Soc. Jpn. **84**, 012001 (2015).

[17] W. Tremel and R. Hoffmann, Square nets of main-group elements in solid-state materials, J. Am. Chem. Soc. **109**, 124 (1987).

[18] Q. Xu, Z. Song, S. Nie, H. Weng, Z. Fang, and X. Dai, Two-dimensional oxide topological insulator with iron-pnictide superconductor LiFeAs structure, Phys. Rev. B **92**, 205310 (2015).

[19] L. M. Schoop, M. N. Ali, C. Straßer, A. Topp, A. Varykhalov, D. Marchenko, V. Duppel, S. S. P. Parkin, B. V. Lotsch, and C. R. Ast, Dirac cone protected by non-symmorphic symmetry and three-dimensional Dirac line node in ZrSiS, Nat. Commun. **7**, 11696 (2016).

[20] M. Neupane, I. Belopolski, M. M. Hosen, D. S. Sanchez, R. Sankar, M. Szlawska, S.-Y. Xu, K. Dimitri, N. Dhakal, P. Maldonado, P. M. Oppeneer, D. Kaczorowski, F. Chou, M. Z. Hasan, and T. Durakiewicz, Observation of topological nodal fermion semimetal phase in ZrSiS, Phys. Rev. B **93**, 201104(R) (2016).

[21] M. Hirayama, R. Okugawa, T. Miyake, and S. Murakami, Topological Dirac nodal lines and surface charges in fcc alkaline earth metals, Nat. Commun. **8**, 14022 (2017).

[22] S. Pezzini, M. R. van Delft, L. M. Schoop, B. V. Lotsch, A. Carrington, M. I. Katsnelson, N. E. Hussey, and S. Wiedmann, Unconventional mass enhancement around the Dirac nodal loop in ZrSiS, Nat. Phys. **14**, 178 (2018).

[23] Y. Shao, A. N. Rudenko, J. Hu, Z. Sun, Y. Zhu, S. Moon, A. J. Millis, S. Yuan, A. I. Lichtenstein, D. Smirnov, Z. Q. Mao, M. I. Katsnelson, and D. N. Basov, Electronic correlations in nodal-line semimetals, Nat. Phys. **16**, 636 (2020).

[24] G. Gatti, A. Crepaldi, M. Puppin, N. Tancogne-Dejean, L. Xian, U. De Giovannini, S. Roth, S. Polishchuk, P. Bugnon, A. Magrez, H. Berger, F. Frassetto, L. Poletto, L. Moreschini, S. Moser, A. Bostwick, E. Rotenberg, A. Rubio, M. Chergui, and M. Grioni, Light-Induced Renormalization of the Dirac Quasiparticles in the Nodal-Line Semimetal ZrSiSe, Phys. Rev. Lett. **125**, 076401 (2020).

[25] B.-B. Fu, C.-J. Yi, T.-T. Zhang, M. Caputo, J.-Z. Ma, X. Gao, B. Q. Lv, L.-Y. Kong, Y.-B. Huang, P. Richard, M. Shi, V. N. Strocov, C. Fang, H.-M. Weng, Y.-G. Shi, T. Qian, and H. Ding, Dirac nodal surfaces and nodal lines in ZrSiS, Sci. Adv. **5**, eaau6459 (2019).

[26] F. Orbanić, M. Novak, Z. Glumac, A. McCollam, L. Tang, and I. Kokanović, Quantum oscillations of the magnetic torque in the nodal-line Dirac semimetal zrsis, Phys. Rev. B **103**, 045122 (2021).

[27] E. Uykur, L. Z. Maulana, L. M. Schoop, B. V. Lotsch, M. Dressel, and A. V. Pronin, Magneto-optical probe of the fully gapped Dirac band in ZrSiS, Phys. Rev. Research **1**, 032015 (2019).

[28] C. S. A. Müller, T. Khouri, M. R. van Delft, S. Pezzini, Y.-T. Hsu, J. Ayres, M. Breitkreiz, L. M. Schoop, A. Carrington, N. E. Hussey, and S. Wiedmann, Determination of the Fermi surface and field-induced quasiparticle tunneling around the Dirac nodal loop in ZrSiS, Phys. Rev. Research **2**, 023217 (2020).

[29] M. Novak, S. N. Zhang, F. Orbanić, N. Biliškov, G. Eguchi, S. Paschen, A. Kimura, X. X. Wang, T. Osada, K. Uchida, M. Sato, Q. S. Wu, O. V. Yazyev, and I. Kokanović, Highly anisotropic interlayer magnetoresitance in ZrSiS nodal-line dirac semimetal, Phys. Rev. B **100**, 085137 (2019).

[30] D. VanGennep, T. A. Paul, C. W. Yerger, S. T. Weir, Y. K. Vohra, and J. J. Hamlin, Possible pressure-induced topological quantum phase transition in the nodal line semimetal ZrSiS, Phys. Rev. B **99**, 085204 (2019).

[31] C. C. Gu, J. Hu, X. L. Chen, Z. P. Guo, B. T. Fu, Y. H. Zhou, C. An, Y. Zhou, R. R. Zhang, C. Y. Xi, Q. Y. Gu, C. Park, H. Y. Shu, W. G. Yang, L. Pi, Y. H. Zhang, Y. G. Yao, Z. R. Yang, J. H. Zhou, J. Sun, et al., Experimental evidence of crystal

symmetry protection for the topological nodal line semimetal state in ZrSiS, Phys. Rev. B **100**, 205124 (2019).

[32] I. M. Lifshitz, Anomalies of Electron Characteristics of a metal in the high pressure region, Zh. Eksp. Teor. Fiz. **38**, 1569 (1960) [Sov. Phys. JETP **11**, 1130 (1960)].

[33] G. P. Mikitik and Y. V. Sharlai, Crossing points of nodal lines in topological semimetals and the Fermi surface of ZrSiS, Phys. Rev. B **101**, 205111 (2020).

[34] G. P. Mikitik, Step-like anomaly of the magnetic susceptibility in crystals with degenerate electronic energy bands, Low Temp. Phys. **33**, 839 (2007).

[35] G. P. Mikitik and Y. V. Sharlai, Magnetic susceptibility of crystals with crossing of their band-contact lines, Low Temp. Phys. **47**, 605 (2021).

[36] Interestingly, the values of these parameters ($v_F \approx 7.7 \times 10^5$ m/s, $B_3 \approx -0.25/m$, $\beta \approx 1.3/m$ where m is the electron mass) roughly estimated in Ref. [33] give $\Delta\chi \approx 6.6 \times 10^{-6}$, which is of the order of $\Delta\chi \approx 9.5 \times 10^{-6}$ (3×10^{-4}emu/mol) presented in Fig. 3(d).

[37] N. Novak, Yuriy V. Sharlai, and Grigorii P. Mikitik (private communication).

[38] N. Kumar, K. Manna, Y. Qi, S.-C. Wu, L. Wang, B. Yan, C. Felser, and C. Shekhar, Unusual magnetotransport from Si-square nets in topological semimetal HfSiS, Phys. Rev. B **95**, 121109(R) (2017).

[39] See Supplemental Material at http://link.aps.org/supplemental/10.1103/PhysRevB.105.L241115 which includes Refs. [40–45].

[40] P. Giannozzi, S. Baroni, N. Bonini, M. Calandra, R. Car, C. Cavazzoni, D. Ceresoli, G. L. Chiarotti, M. Cococcioni, I. Dabo *et al.*, QUANTUM ESPRESSO: A modular and open-source software project for quantum simulations of materials, J. Phys.: Condens. Matter **21**, 395502 (2009).

[41] P Giannozzi Jr, O. Andreussi, T. Brumme, O. Bunau, M. B. Nardelli, M. Calandra, R. Car, C. Cavazzoni, D. Ceresoli, M. Cococcioni *et al.*, Advanced capabilities for materials modelling with quantum ESPRESSO, J. Phys.: Condens. Matter **29**, 465901 (2017).

[42] P. Giannozzi, O. Baseggio, P. Bonfà, D. Brunato, R. Car, I. Carnimeo, C. Cavazzoni, S. de Gironcoli, P. Delugas, F. Ferrari Ruffino, A. Ferretti, N. Marzari, I. Timrov, A. Urru, and S. Baroni, Quantum Espresso toward the exascale, J. Chem. Phys. **152**, 154105 (2020).

[43] J. P. Perdew, A. Ruzsinszky, G. I. Csonka, O. A. Vydrov, G. E. Scuseria, L. A. Constantin, X. Zhou, and K. Burke, Restoring the Density-Gradient Expansion for Exchange in Solids and Surfaces, Phys. Rev. Lett. **100**, 136406 (2008).

[44] M. J. van Setten, M. Giantomassi, E. Bousquet, M. J. Verstraete, D. R. Hamann, X. Gonze, and G.-M. Rignanese, The pseudodojo: Training and grading a 85 element optimized norm-conserving pseudopotential table, Comput. Phys. Commun. **226**, 39 (2018).

[45] N. Marzari, D. Vanderbilt, A. De Vita, and M. C. Payne, Thermal Contraction and Disordering of the Al(110) Surface, Phys. Rev. Lett. **82**, 3296 (1999).